Available online at www.sciencedirect.com
ScienceDirect
Acta Materialia 57 (2009) 116–124
Acta MATERIALIA
www.elsevier.com/locate/actamat

Phase-field simulations of $\alpha \rightarrow \gamma$ precipitations and transition to massive transformation in the Ti–Al alloy

H.M. Singer [a,*], I. Singer [b], A. Jacot [a]

[a] *Laboratoire de Simulation des Matériaux LSMX, Ecole Polytechnique Fédérale de Lausanne EPFL, EPFL STI IMX LSMX, Station 12, CH–1015 Lausanne, Switzerland*

[b] *Department of Mechanics, Royal Institute of Technology KTH, SE-10044, Stockholm, Sweden*

Received 30 October 2007; received in revised form 28 August 2008; accepted 29 August 2008
Available online 1 October 2008

Abstract

A phase-field model for the solid–solid $\alpha \rightarrow \gamma$ transition of Ti–Al binary alloys is presented based on analytical Gibbs free energies and couplings to the thermodynamical database ThermoCalc. The equilibrium values recover the $\alpha + \gamma$ phase boundaries. Morphological transitions from diffusive to massive (partitionless) growth are observed on increasing the initial mole fraction of aluminum. Temporal evolution of the interface shows a $\sqrt{t}$ behavior for diffusive and a linear behavior for massive growth, which is in accordance with theoretical predictions. An estimate of the interfacial mobility of Ti–Al based on the Burke–Turnbull equation is calculated. The expression of the mobility follows an Arrhenius law. Using the derived interfacial mobility, the calculated interfacial velocities of the massive transformation are in quantitative agreement with those observed in experiments.

Keywords: Phase-field models; Titanium aluminides; Phase transformations; Mobility; Modeling

1. Introduction

Gamma titanium aluminides have been the subject of considerable interest in recent years. Due to their attractive properties, high-temperature applications in aerospace and automotive industries are considered. These alloys show a fine, lamellar microstructure. They provide higher yield strength than Ti-based alloys and at the same time a low density, a high specific stiffness and an excellent oxidation resistance at elevated temperatures as well as good creep properties [1–4].

It is well established that there is a strong correlation between the formed microstructures and the final mechanical properties of a material, and thus many experimental studies on the phase transformations have been performed (e.g. [5,6] and references therein, [7,8]), especially during the solid–solid transformations in the course of heat treatments [9,10].

Phase-field models for different phase transformations of Ti–Al alloys have been proposed. Guo et al. [11] have used a KKS model [12] to simulate directional solidification of a $Ti_{55}Al_{45}$ alloy with the free energy derived from Calphad thermodynamic modeling. Wen et al. [13] introduced a three-dimensional phase-field model for the $\alpha_2' \rightarrow \alpha_2 + \gamma$ solid–solid transformation, which takes into account coherency strain associated with the lattice rearrangement. Lamellar structures similar to the experimental structures were found. The influence of the coherency strain was claimed to be the dominating factor for the formation of lamellae. A model taking also into account stacking faults at intermediate stages and heterogeneous nucleation of the γ phase was developed by Katzarov et al. [14], who based their model derivation on the stress methodology used in Wang and Khatchaturyan [15].

In this paper a phase-field model is presented, which concentrates on the dynamics of the Ti–Al system; in particular the transition from diffusive to massive growth is investigated in the framework of analytical Gibbs free energies and coupling to thermodynamical databases such as

* Corresponding author.
E-mail address: hsinger@solid.phys.ethz.ch (H.M. Singer).

1359-6454/$34.00
doi:10.1016/j.actamat.2008.08.055

ThermoCalc. In Section 2.1 the mathematical background of the model is briefly introduced. In Section 2.2 details on the modeling of the Gibbs free energy are presented. Details on the implementation and the coupling to thermodynamical data bases are given in Sections 2.3 and 2.4. In Section 3 we present the results of the model calculations: equilibrium calculations show that the model recovers to the exact phase boundaries of the $\alpha+\gamma$ region; measurements of the dynamic system behavior, in particular the interface velocity, show the transition from diffusive to massive growth. Based on this model, an estimate of the interfacial mobility is presented. Finally in Section 4 the obtained results are discussed and a brief conclusion is given.

2. Phase field model

2.1. General model description

The phase-field model of $\alpha \rightarrow \gamma$ phase transition in Ti–Al alloy is based on the model of Singer-Loginova et al. [16,17], who introduced a Gibbs free energy functional of a solid–solid transformation in a binary alloy

$$G = \int_{\Omega} \left(\frac{G_m(x_{\mathrm{Al}}, \phi, T)}{V_m} + \frac{\varepsilon^2}{2} |\nabla \phi|^2 \right) \mathrm{d}\Omega \tag{1}$$

where G_m denotes the molar Gibbs free energy and V_m is the molar volume and is assumed to be constant. x_{Al} is the mole fraction of aluminum. The variable ϕ is the phase field, which takes values of 1 in the γ-phase and *0* in the α-phase and varies smoothly between those values over the phase boundary. Due to rapid heat conduction, isothermal conditions of the temperature T for the whole domain are assumed.

The interfacial energy of the system σ enters in the free energy functional of Eq. (1) by the parameter ε, which is related to the interface thickness δ [18] as

$$\varepsilon^2 = 3\sqrt{2}\sigma\delta. \tag{2}$$

The molar free energy G_m is constructed as a mixture of the molar free energies in the α and γ phases, respectively, and an additional energy hump [19]:

$$G_m = (1 - p(\phi)) G_m^{\alpha} + p(\phi) G_m^{\gamma} + g(\phi) W \tag{3}$$

where $W = 6\sigma V_m/\sqrt{2}\delta$ is the height of the energy hump and $g(\phi)$, $p(\phi)$ are the standard phase-field polynomial functions:

$$g(\phi) = \phi^2 (1-\phi)^2 \tag{4}$$

$$p(\phi) = \phi^3 (10 - 15\phi + 30\phi^2) \tag{5}$$

The phase-field equation is derived by the variational Allen–Cahn formalism:

$$\frac{\partial \phi}{\partial t} = -M_{\phi} \frac{\delta G}{\delta \phi} \tag{6}$$

$$\frac{\partial \phi}{\partial t} = M_{\phi} \left(\varepsilon^2 \nabla^2 \phi + \frac{1}{V_m} \left(p'(\phi) \left(G_m^{\alpha} - G_m^{\gamma} \right) - g'(\phi) W \right) \right). \tag{7}$$

where p' and g' are the derivatives with respect to ϕ and M_{ϕ} is related to the interfacial mobility M as $M_{\phi} = 0.235 M/\delta$ [16].

The derivation of the diffusion equation is rather cumbersome. While here we present only an outline, the detailed derivation is given in Appendices B and C. The evolution of the concentration field is governed by the normal diffusion equation:

$$\frac{\partial x_{\mathrm{Al}}}{\partial t} = -\nabla \cdot \mathbf{J}_{\mathrm{Al}} \tag{8}$$

The diffusional flux of aluminum is given by Onsager's law and can be expanded in terms of the concentration and the phase-field gradients:

$$\mathbf{J}_{\mathrm{Al}} = -L'' \nabla \left(\frac{\delta G_m}{\delta x_{\mathrm{Al}}} \right) \tag{9}$$

$$\mathbf{J}_{\mathrm{Al}} = -L'' \nabla \left(\frac{\partial^2 G_m}{\partial x_{\mathrm{Al}}^2} \nabla x_{\mathrm{Al}} + \frac{\partial^2 G_m}{\partial x_{\mathrm{Al}} \partial \phi} \nabla \phi \right) \tag{10}$$

where the kinetic parameter L'' is related to the diffusional mobility of aluminum M_{Al}, which is modeled as a function of the phase-field variable. For a disordered α-phase one can write $L'' = x_{\mathrm{Al}}(1 - x_{\mathrm{Al}}) M_{\mathrm{Al}}$, while the expression of L'' for the ordered γ-phase is more complicated and is given in Appendix C. Combined, the diffusion equation is written as

$$\frac{\partial x_{\mathrm{Al}}}{\partial t} = \nabla \cdot \left(L''(x_{\mathrm{Al}}, \phi) \left(\frac{\partial^2 G_m}{\partial x_{\mathrm{Al}}^2} \nabla x_{\mathrm{Al}} + \frac{\partial^2 G_m}{\partial x_{\mathrm{Al}} \partial \phi} \nabla \phi \right) \right). \tag{11}$$

2.2. The Ti–Al system

In the last decade intensive experimental investigations of the Ti–Al phase equilibria have been performed (e.g. [20–22]). In parallel thermodynamic descriptions of the Ti–Al system have successively improved to match the experimental results [23,24]. Zhang et al. [25] have made great efforts to describe the Gibbs energy of the ordered phases of Ti–Al. Ohnuma et al. [26] provided new experimental data and reported a thermodynamic analysis that takes into account the ordering configurations in several phases. The criticism was raised that the model calculations of Zhang et al. described the Gibbs energies of the ordered and disordered phases with the same primitive structure independently. Nevertheless the calculations were in excellent agreement with the experimental results. For our numerical phase-field simulations we have decided to use the Gibbs energies of Zhang et al. [25] for the ordered and disordered phases γ and $\alpha+\gamma$, respectively.

The Gibbs energy of the disordered solutions phases is given by [25]:

$$G_m = x_{\mathrm{Ti}}{}^0 G_{\mathrm{Ti}} + x_{\mathrm{Al}}{}^0 G_{\mathrm{Al}} + RT(x_{\mathrm{Ti}} \ln x_{\mathrm{Ti}} + x_{\mathrm{Al}} \ln x_{\mathrm{Al}}) + x_{\mathrm{Ti}} x_{\mathrm{Al}} [G_0 + G_1 (x_{\mathrm{Ti}} - x_{\mathrm{Al}})] \tag{12}$$

where x_i is the mole fraction of component i and ${}^0G_i$ is the Gibbs energy of a component in its standard state. The first

two terms on the right-hand side describe the mechanical mixture of the components, the third term the ideal Gibbs energy of mixing and the fourth term the excess Gibbs energy. The parameters G_0 and G_1 were obtained by optimization.

The Gibbs energy of ordered phases is described with a generalized bond-energy model [25,27]:

$$G_m = x_{\mathrm{Ti}}{}^0G_{\mathrm{Ti}} + x_{\mathrm{Al}}{}^0G_{\mathrm{Al}} + \sum_{i=1}^{2}\sum_{i=1}^{2}(V_{12}Z^{ij} + \widetilde{V}_{12}\widetilde{Z}^{ij})X^i y^i_{\mathrm{Ti}} y^j_{\mathrm{Al}} + RT\sum_{i=1}^{2} X^i(y^i_{\mathrm{Ti}}\ln y^i_{\mathrm{Ti}} + y^j_{\mathrm{Al}}\ln y^j_{\mathrm{Al}}) \quad (13)$$

where X^i ($i = 1,2$) is the site fraction of the sublattice i relative to the total lattice sites and y^i_p is the concentration of the component p on sublattice i, Z^{ij} and $\widetilde{Z}^{ij}$ are the numbers of the first nearest neighbors and the second nearest neighbors on sublattice j (i, $j = 1$, 2), V_{12} represents the interchange energy between the first nearest neighbors and $\widetilde{V}_{12}$ the interchange energy between the second nearest neighbors with $\widetilde{V}_{12} = aV_{12}$ and $a = \mathrm{const}$.

In Ref. [25], it is argued that within experimental errors a linear relationship $A + BT$ for the free energy is sufficient to represent the energy differences between various states, as opposed to Dinsdale [28], who used the complex expression $a + bT + cT\ln + dT^2 + e/T + fT^3 + gT^4 + hT^7 + iT^{-9}$ with $a, \ldots, i$, A, B as constants.

The standard state formulations for ${}^0G_{\mathrm{Al}}$ and ${}^0G_{\mathrm{Ti}}$ [29] are given in Appendix A as functions of the temperature. The full free energies for α and γ Ti–Al and their concentration dependence are given in Appendix B.

2.3. Numerical evaluation

In order to solve Eqs. (7) and (11) numerically several possible methods have been proposed. It is possible to solve them (in principle) with a explicit finite difference method with forward Euler time stepping. However, even for the one-dimensional case with realistic interface thicknesses of the order of nanometers and a reasonable mesh of the order of 5000–10000 grid nodes the calculation times become rather lengthy. Implicit methods such as backward Euler scheme are unconditionally stable and seem to have offer large advantages over the explicit ones [16]. However the implementation for implicit solvers is non-trivial. In the literature different numerical methods have been used for spatial discretization of the phase-field equations: finite elements (FEM) [30,31], finite volumes (FV) [32,33], especially for the simulation of two- and three-dimensional structures. FEM and FV formulations have the additional advantage of allowing spatial adaptivity.

In this paper we have used a fourth-order Runge-Kutta approach for the time integration. While still being explicit in time with almost the same stability criterion as for forward Euler, the time step can be increased by more than an order of magnitude. Interestingly, this approach, despite its practical usefulness and ease of implementation, has to our knowledge hardly been used for phase-field simulations [34,35].

2.4. Coupling to thermodynamical databases

While the analytical derivation of the model with the Gibbs free energy was used to prove the validity of the model, it was found that this description, although very general, restricts the possible uses of the proposed model. The model parameters y^i_p have to be precalculated for every temperature T separately by the optimization process described in Ref. [25]. Moreover, the analytical derivation requires precise expressions for the diffusional and interfacial mobilities, which to the authors' knowledge are not available for Ti–Al alloy. In general, the expressions of the Gibbs energies and the mobilities are only known for a limited number of alloys (e.g. Fe–C [36]), which typically leads to extremely complicated mathematical expression of phase-field models (see Appendices A–C).

Therefore, especially for use in industrial applications, it is favorable to rely on thermodynamic databases such as ThermoCalc, which furnish numerical values for the Gibbs energies of the alloy of interest. We note, however, that a direct coupling of the phase-field simulations with the ThermoCalc database is unsatisfactory for two reasons: (i) it is very inefficient in terms of access times for a requested value, and (ii) it creates strong dependencies on a specific product.

Instead of the direct coupling with the ThermoCalc data base we have used precalculated values for $G_\alpha(x_{\mathrm{Al}}, T)$ and $G_\gamma(x_{\mathrm{Al}}, T)$ in the range $x_{\mathrm{Al}} = 0.365,\ 0.370, \ldots, 0.52$ and $T = 773,\ 778, \ldots, 1673$ K. Internally the data for the Gibbs energies is calculated by the Redlich–Kistler polynomials (e.g. [37]). We have found, however, that in the range relevant for the phase-field simulations, the numerical data can be accurately approximated by nth order polynomials, where $n = 6$–8, as a function of the concentration for a given temperature. The polynomials have the advantage of being easily analytically differentiable, so that no numerical artifacts are introduced. Furthermore the polynomial fits can be precalculated and stored in a table for easy access during the simulations. So far, we have performed simulations for constant temperatures. However, this approach is easily extendable by interpolation to changes in temperatures during the simulations in order to consider the effects of heat treatments or continuous cooling. In Fig. 1 the position of the phase boundary as a function of time for diffusive growth is shown, calculated by the analytical and numerical Gibbs energies at 700 °C. A good agreement between the analytical description and the data obtained from ThermoCalc is found.

The results presented in the following section were obtained by direct use of Eq. (11) instead of the analytical Eq. (50) in Appendix C. The simulation parameters are given in Table 1.

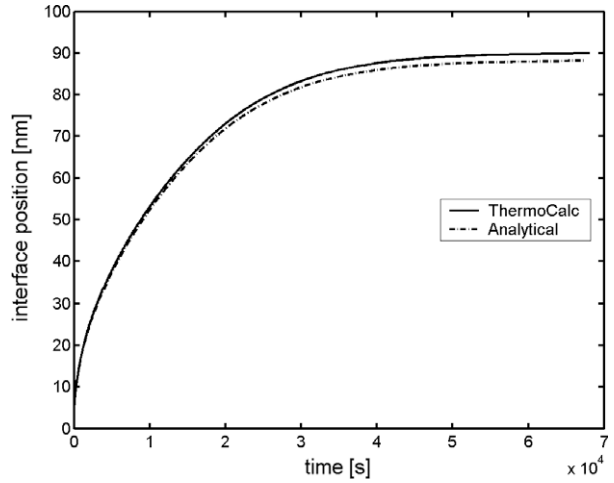

Fig. 1. Interface position given by the analytical description (dashed line) (see Appendices A–C) and the numerical data obtained by ThermoCalc. The simulations were performed at $T = 700$ °C and an initial concentration of $x_{Al} = 0.4$ in a domain of 250 nm.

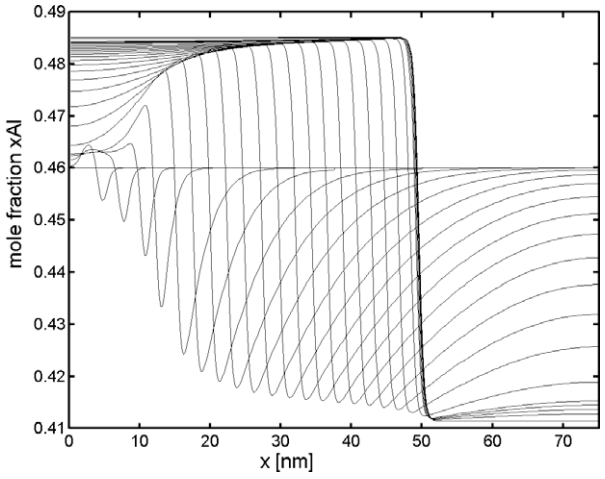

Fig. 2. Relaxation to equilibrium concentrations. The diffusional depletion is rearranging to a step function between the α- and the γ-phase. The simulations are performed at $T = 1145$ °C and initial concentration $x_{Al,0} = 0.46$. The mole fraction profiles are shown at different times: $t = 10^{-7}$, $1.5 \cdot 10^{-6}$, $4.5 \cdot 10^{-6}$,…, $1.4 \cdot 10^{-2}$, 3.7 s.

3. Results

3.1. Equilibrium: quantitative recovery of the phase diagram

In order to test the quantitative prediction capabilities of the proposed model, we have calculated equilibrium concentration profiles for the $\alpha \rightarrow \gamma$ transition and compared the results to the phase boundary data obtained by ThermoCalc. The initial condition for the simulations is homogeneous α with a very thin layer of γ formed at the left side of the system. In Fig. 2, the relaxation to the equilibrium profile is shown for the temperature $T = 1145$ °C. Initially a bump behind the depletion is created, which, as time increases, will relax to the equilibrium concentration.

Calculating the phase boundaries for the $\alpha + \gamma$ region with the presented phase-field model we have found that the deviation from the ThermoCalc data was in every calculated case less than 10^{-3}.

3.2. Dynamics of the system

3.2.1. Morphological transition: diffusion to massive growth

A qualitatively different behavior of the phase transformation can be found for different initial concentrations. A space time plot for diffusive growth is shown in Fig. 3a. On increase of the concentration at constant temperatures, the system changes to massive growth in Fig. 3b. The interfacial velocity increases drastically. In diffusive growth the interface propagates with a $\sqrt{t}$ dependence until the impingement of the diffusion boundary layer with the domain boundary sets in. For the massive growth, the velocity becomes constant, and thus the interface position propagates linearly in time. In Fig. 4, the interface position is plotted as a function of time for different initial concentrations, which demonstrates the behavioral change of the system on this morphological transition.

Table 1
Simulation parameters for the phase-field calculations

Interface thickness	δ[nm]	1
Molar volume	V_m [m^3/mol]	$10.1 \cdot 10^{-6}$
Interfacial energy	σ [J/m^2]	0.3
Al-diffusion [38–41]	D_{Al} [m^2/s]	$6.65 \cdot 10^{-3} \exp(\frac{-329000}{RT})$
Ti-diffusion [38–41]	D_{Ti} [m^2/s]	$1.35 \cdot 10^{-3} \exp(\frac{-303000}{RT})$

The data for the Gibbs free energies are given in the Appendix.

3.2.2. Prediction of interfacial mobility

While the equilibrium behavior in the limit is not sensitive to the mobility of the interface, the dynamics of the system is far less quantitative since accurate physical values in Ti–Al for the interfacial mobilities are to the best of our knowledge not known. However, in order to study the morphological behavior of the system especially in two and three dimensions, a dependence of the interfacial mobility on the temperature must be derived. Based on thermodynamic considerations a partitionless transformation becomes possible in this system only at temperatures below the T_0 line, which is the temperature at which the free energies of the α- and γ-phase are equal. However, the exact temperature at which such a transformation becomes kinetically possible is still a matter of controversy. An extensive review on this debate is given in Ref. [42]. In the present study, we have investigated three scenarios:

(i) First, we assumed that the transition between diffusive and massive growth occurs exactly at the T_0 line. Then, for a given temperature, we have calculated the T_0-concentration and by performing multiple simulations we have found a value for the interfacial mobility that produces diffusive and massive growth at the T_0-concentration and just slightly above it (i.e. slightly below the T_0 temperature), respectively. By performing the above procedure for every acceptable temperature we were able to find values for the

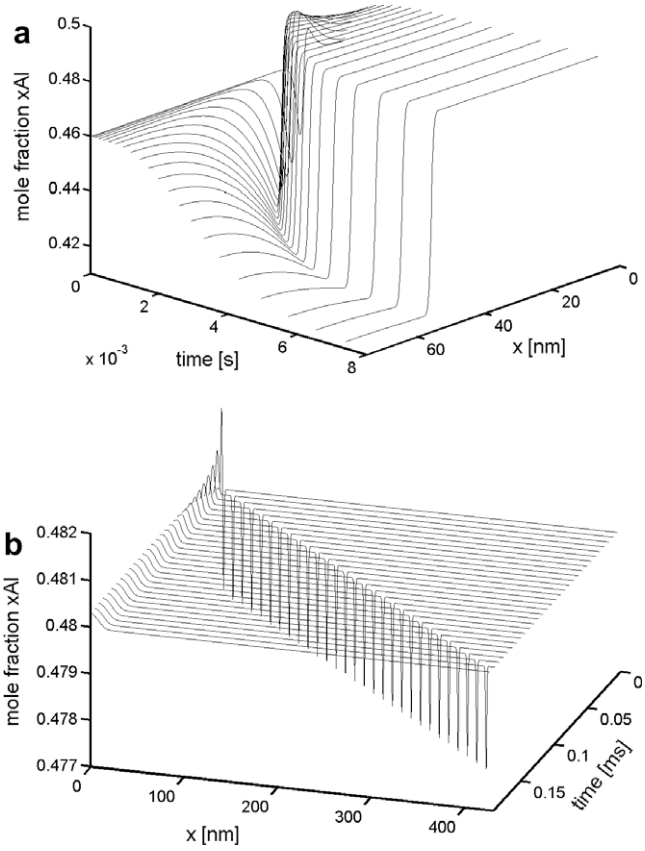

Fig. 3. Two-dimensional space–time plot of (a) diffusive phase transformation, (b) massive phase transformation with constant velocity of the interface. The simulations were performed at $T = 1145\,^{\circ}\mathrm{C}$ and (a) $x_{\mathrm{Al},0} = 0.46$ for diffusive growth, where the concentration profiles are given at different instances $t = 0, 0.02, 0.07, 0.14, \ldots, 6.5, 7.4$ ms and a total simulation time is $t_{\mathrm{end}} = 7.4$ ms and (b) $x_{\mathrm{Al},0} = 0.48$ for massive growth, where each line is separated by a time increment of $\Delta t = 6.6$ μs and the total simulation time is $t_{\mathrm{end}} = 0.19$ ms. The notch value, corresponding to the concentration at the phase interface, is 0.4774.

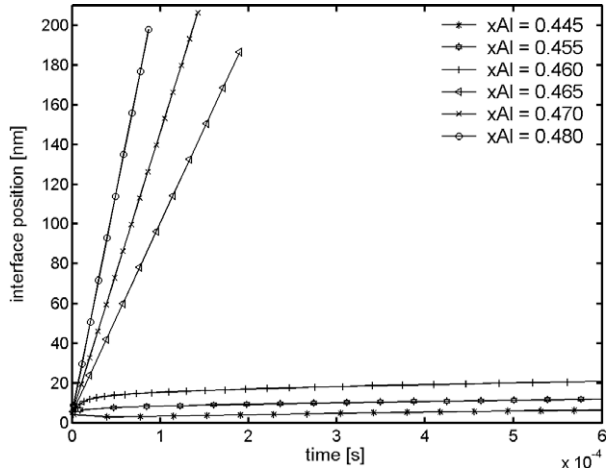

Fig. 4. Position of the interface as a function of time for different initial concentrations with superimposed square-root fit for diffusive growth and linear fit for massive growth.

interfacial mobility (line A in Fig. 6), which follow an Arrhenius law.

$$M_{\mathrm{A}} = 370 \cdot \exp\left(\frac{-38916}{T}\right) \mathrm{m}^4\,\mathrm{J}^{-1}\,\mathrm{s}^{-1}. \tag{14}$$

However, the interfacial velocities of the massive transformations turned out to be approximately one order of magnitude larger than those found experimentally [43] and predicted by the Burke–Turnbull equation [44].

(ii) For a given concentration the Burke–Turnbull equation [43,44] specifies the growth velocity V of the interface as a function of the temperature (see Fig. 5) during massive transformation for an interface-controlled reaction

$$V = 23020\left(\frac{-(G_m^{\alpha} - G_m^{\gamma})}{RT}\right) exp\left(\frac{-155250}{RT}\right). \tag{15}$$

In this equation the activation enthalpy and activation entropy of the original Burke–Turnbull equation for interface diffusion were already measured by Veeraraghavan et al. [43] and replaced by numerical values. We have assumed that the critical temperature below which the transition to massive transformation becomes possible corresponds to the maximum of the Burke–Turnbull plot. Then, for every acceptable concentration, we have repeated the procedure described in (i) and found an expression for the interfacial mobility shown as line B in Fig. 6

$$M_{\mathrm{B}} = 5.98 \cdot 10^{-3} \exp\left(\frac{-27947}{T}\right) \mathrm{m}^4\,\mathrm{J}^{-1}\,\mathrm{s}^{-1}. \tag{16}$$

With this mobility the interfacial velocities of the massive transformation are underestimated by a factor of 6 compared to those found experimentally [43].

(iii) For every concentration and temperature corresponding to the maximum of the Burke–Turnbull plot we have tuned the interfacial mobility to produce the maximum interfacial velocity predicted by the Burke–Turnbull equation. The obtained mobility is shown in Fig. 6 as line C. Its expression is

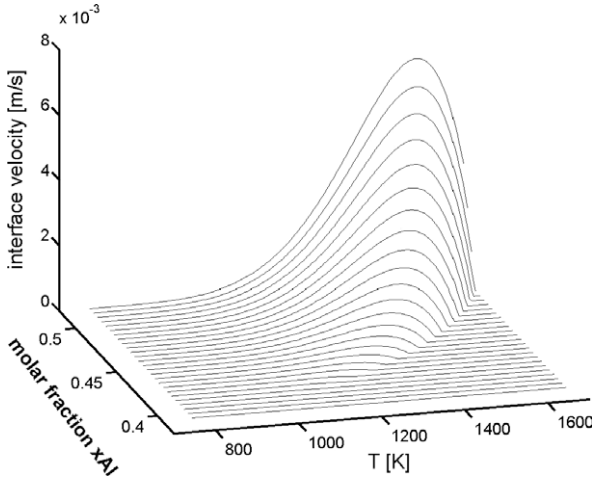

Fig. 5. The interfacial velocity of the massive transformation predicted by the Burke–Turnbull equation Eq. (15) as a function of temperature and mole fraction.

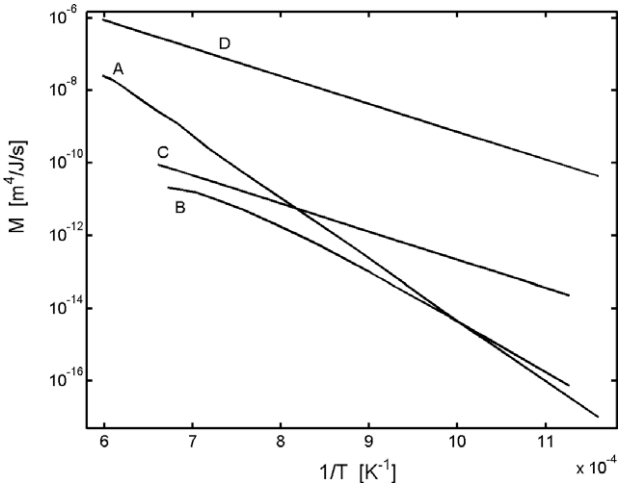

Fig. 6. Interfacial mobility coefficients as a function of $1/T$ calculated (A) based on the assumption that a morphology transition from diffusive to massive growth occurs at the T_0 line of the phase diagram, (B) based on the assumption that the morphology transition from diffusive to massive growth for a given mole fraction occurs at the temperature corresponding to the maximum of the Burke–Turnbull plot (Fig. 5), (C) as a fit to the maximum growth velocity predicted by the Burke–Turnbull equation. (D) The interfacial mobility of the Fe–C alloy is included for comparison.

$$M_C = 1.24 \cdot 10^{-5} \exp\left(\frac{-17847}{T}\right) \mathrm{m}^4\ \mathrm{J}^{-1}\ \mathrm{s}^{-1}. \qquad (17)$$

With the interfacial mobility M_C we have performed simulations of massive growth at $x_{Al} = 0.475$ and different temperatures. The obtained interfacial velocities are in quantitative agreement with the experimental observation as demonstrated in Fig. 7. We should note, however, that the data for the Gibbs energies used in Ref. [43] differs from ours, which explains the slight right shift of the experimental data with respect to the analytical Burke–Turnbull equation. Additionally, we have calculated the transition

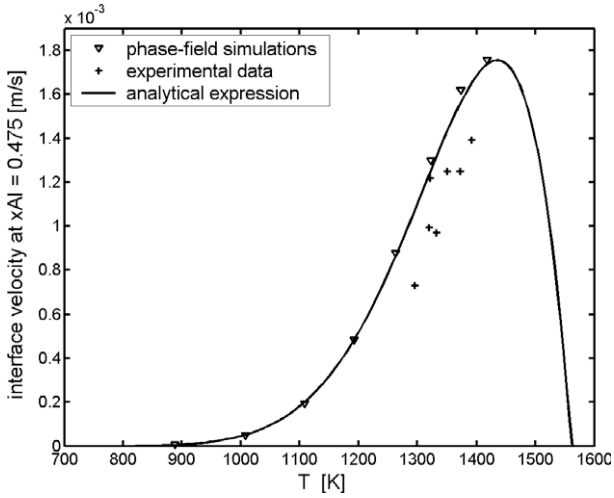

Fig. 7. Comparison of the calculated interfacial velocity for $x_{Al} = 0.475$ and different temperatures with the analytical prediction of the Burke–Turnbull equation and experimental data from Ref. [43]. The interfacial velocities are calculated with the interfacial mobility Eq. (17) shown as line C in Fig. 6.

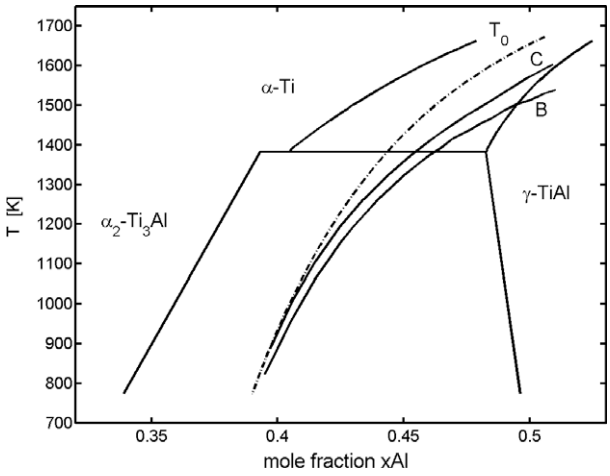

Fig. 8. A portion of the Ti–Al phase diagram with superimposed T_0 line (dashed-dotted line). The black lines demonstrate the critical compositions above which transition from diffusive to massive growth becomes possible for a given temperature. The lines B and C correspond to the interfacial mobility M_B Eq. (16) and M_C, Eq. (17) respectively.

border from diffusive to massive transformations shown as lines B and C in Fig. 8. As can be seen from Fig. 8, the morphological transition occurs below the T_0 line, as predicted thermodynamically [42].

For comparison, the known values for the interfacial mobility in the Fe–C system [45] are plotted in Fig. 6 as line D. The big difference in values between line D and lines A–C might be explained by the fact that diffusional mobilities in Fe–C change only by 3 orders of magnitude, while in the Ti–Al system the change is by 10 orders of magnitude (Table 1) in the range of temperatures investigated.

4. Discussion and conclusions

A phase-field model for $\alpha \rightarrow \gamma$ solid–solid phase transformation in Ti–Al is presented. The model is capable of predicting the behavior of the diffusion field for the whole range of concentrations and temperatures corresponding to the $\alpha + \gamma$ region of the Ti–Al phase diagram. We have presented a detailed analytical description of the model and demonstrated that the simulations recover accurately the equilibrium values of the phase diagram. However, the available analytical description of the Gibbs energy is accurate only at low temperatures. We have presented a coupling to the ThermoCalc database and shown that for a given temperature the system can undergo either diffusion-controlled or massive transformation depending on the initial Al content of the α-phase. By fitting values of the interfacial mobility to produce maximum velocities predicted by the Burke–Turnbull equations we have derived an estimate for the interfacial mobility as a function of the temperature. The derived expression follows an Arrhenius law and produces results that are in good quantitative agreement with the experimental data.

Our intention is to extend the simulations to higher dimensions in order to investigate morphological changes,

which Ti–Al undergoes during different heat treatments as was found in experimental studies [5,6].

Acknowledgements

H.M.S. express his foremost gratitude to Dr. U.R. Kattner (NIST) for her most useful and valuable discussions and help with the Ti–Al free energies. The authors also would like to thank Dr. M. Gasik (Helsinki Institute of Technology) and Dr. M. Selleby (KTH, Stockholm). Valuable discussions with A. Rostamian, EPFL are gratefully acknowledged. This work is financially supported by the European Commission (Contract No. NMP-CT-2004-500635) 6th Framework Program as the project "Intermetallic Materials Processing in Relation to Earth and Space Solidification", which is co-funded and coordinated by the European Space Agency, with additional project funding contributions from the Government of Switzerland.

Appendix A. Thermodynamic data of Ti–Al

The free energy formulations in the standard states for ${}^0G_{\mathrm{Al}}$ and ${}^0G_{\mathrm{Ti}}$ [29] are given by

$$\begin{aligned}{}^0G_{\mathrm{Al}}^{\mathrm{hcp}} = & -7976.15 + 137.071542T - 24.3671976T\ln(T) \\ & - 11277.683 + 188.661987T - 31.748192T\ln(T) \\ & - 1.234264\cdot 10^{28}T^{-9} + 5481 - 1.8T \end{aligned} \tag{18}$$

for 933.6–2900 K and

$$\begin{aligned}{}^0G_{\mathrm{Ti}}^{\mathrm{fcc}} = & -8059.921 + 133.687208T - 23.9933T\ln(T) \\ & + 908.837 + 67.048538T - 14.9466T\ln(T) \\ & - 0.0081465T^2 + 2.02715\cdot 10^{-7}T^3 \\ & - 1477660T^{-1} + 6000 - 0.1T \end{aligned} \tag{19}$$

in the temperature range 1155–1941 K and

$$\begin{aligned}{}^0G_{\mathrm{Ti}}^{\mathrm{fcc}} = & -8059.921 + 133.687208T - 23.9933T\ln(T) \\ & - 7811.815 + 133.060068T - 23.9887T\ln(T) \\ & - 0.0042033T^2 - 9.0876\cdot 10^{-8}T^3 + 42680T^{-1} \\ & + 6000 - 0.1T \end{aligned} \tag{20}$$

for 900–1155 K.

Appendix B

The free energies G_m^{α} and G_m^{γ} are given by the disordered and ordered solutions (generalized bond-energy model [25,27]) in Eqs. (12) and (13), respectively. The numerical values [25] used for the α-phase are $G_0 = -123476.4 + 27.38338T$ and $G_1 = -16484.1 + 3.74935T$. The numerical values for the γ-phase are $V_{12} = 2900.3 - 4.25469T - (26871.2 - 17.17261T)x_{\mathrm{Al}} + (22047.2 - 14.44646T)x_{\mathrm{Al}}^2$ and $Z^{11} = 4, Z^{12} = 8, Z^{21} = 8, Z^{22} = 4$, $\widetilde{Z}^{11} = 6, \widetilde{Z}^{12} = 16, \widetilde{Z}^{21} = 16, \widetilde{Z}^{22} = 6$ and $a = 0.6$. The stoichiometric coefficients are $X^1 = X^2 = 1/2$.

According to the generalized bond-energy model [27], there are six variables in G_m^{γ}; however, only two of them are independent. We will use x_{Al} and y_{Al}^1 as being independent. Therefore

$$x_{\mathrm{Ti}} = 1 - x_{\mathrm{Al}} \tag{21}$$

$$y_{\mathrm{Al}}^2 = \frac{1}{X^2}(x_{\mathrm{Al}} - X^1 y_{\mathrm{Al}}^1) = 2x_{\mathrm{Al}} - y_{\mathrm{Al}}^1 \tag{22}$$

$$y_{\mathrm{Ti}}^1 = 1 - y_{\mathrm{Al}}^1 \tag{23}$$

$$y_{\mathrm{Ti}}^2 = 1 - y_{\mathrm{Al}}^2 \tag{24}$$

According to Kattner [29], the order parameter y_{Al}^1 can be, in a first-order approximation, written as

$$x_{\mathrm{Al}} \leqslant 0.5 : y_{\mathrm{Al}}^1 = 0, y_{\mathrm{Al}}^2 = 2x_{\mathrm{Al}} \tag{25}$$

$$x_{\mathrm{Al}} > 0.5 : y_{\mathrm{Al}}^1 = 2x_{\mathrm{Al}} - 1, y_{\mathrm{Al}}^2 = 1 \tag{26}$$

Therefore

$$x_{\mathrm{Al}} \leqslant 0.5 : y_{\mathrm{Ti}}^1 = 1, y_{\mathrm{Ti}}^2 = 1 - 2x_{\mathrm{Al}} \tag{27}$$

$$x_{\mathrm{Al}} > 0.5 : y_{\mathrm{Ti}}^1 = 2(x_{\mathrm{Al}} - 1), y_{\mathrm{Ti}}^2 = 0 \tag{28}$$

These values are accurate for 700 °C. For different temperatures the data must be recalculated by optimizing ([25]).

For the case $x_{\mathrm{Al}} \leqslant 0.5$ we find

$$\begin{aligned} G_m^{\gamma} = & (1-x_{\mathrm{Al}})\,{}^0G_{\mathrm{Ti}}^{\gamma} + x_{\mathrm{Al}}\,{}^0G_{\mathrm{Al}}^{\gamma} + \frac{1}{2}RT[2(1-x_{\mathrm{Al}})\ln(2(1-x_{\mathrm{Al}})) \\ & + (2x_{\mathrm{Al}}-1)\ln(2x_{\mathrm{Al}}-1)] + \frac{1}{2}A^{11}(2(1-x_{\mathrm{Al}})(2x_{\mathrm{Al}}-1) \\ & + \frac{1}{2}A^{22}2(1-x_{\mathrm{Al}})) \end{aligned} \tag{29}$$

and for $x_{\mathrm{Al}} > 0.5$

$$\begin{aligned} G_m^{\gamma} = & (1-x_{\mathrm{Al}})\,{}^0G_{\mathrm{Ti}}^{\gamma} + x_{\mathrm{Al}}\,{}^0G_{\mathrm{Al}}^{\gamma} + \frac{1}{2}RT[(1-2x_{\mathrm{Al}})\ln(1-2x_{\mathrm{Al}}) \\ & + 2x_{\mathrm{Al}}\ln(2x_{\mathrm{Al}})] + \frac{1}{2}(A^{12}(2x_{\mathrm{Al}}) + A^{22}(1-2x_{\mathrm{Al}})2x_{\mathrm{Al}}) \end{aligned} \tag{30}$$

with $A^{ij} = A^{ij}(x_{\mathrm{Al}}, T) = (V_{ij}Z^{ij} + \widetilde{V}_{ij}\widetilde{Z}^{ij})$.

The Gibbs free energy in the α-phase is given by

$$\begin{aligned} G_m^{\alpha} = & (1-x_{\mathrm{Al}})\,{}^0G_{\mathrm{Ti}}^{\alpha} + x_{\mathrm{Al}}\,{}^0G_{\mathrm{Al}}^{\alpha} + RT[(1-x_{\mathrm{Al}})\ln(1-x_{\mathrm{Al}}) \\ & + x_{\mathrm{Al}}\ln x_{\mathrm{Al}} + (1-x_{\mathrm{Al}})(G_0^{\alpha} + G_1^{\alpha}(1-2x_{\mathrm{Al}})) \end{aligned} \tag{31}$$

Appendix C

Here, we give the derivation for the diffusion equations in terms of the free energies in Eqs. (29)–(31).

The diffusion equation is given by

$$\dot{x}_{\mathrm{Al}} = -\nabla\cdot\mathbf{J}_{\mathrm{Al}} \tag{32}$$

$$\mathbf{J}_{\mathrm{Al}} = -L''\nabla\left(\frac{\delta G_m}{\delta x_{\mathrm{Al}}}\right) \tag{33}$$

where L'' is a phenomenological constant usually modeled as $L'' = x_{\mathrm{Al}}(1-x_{\mathrm{Al}})M_{\mathrm{Al}}$ with M_{Al} the diffusional mobility. It follows immediately

$$\nabla\left(\frac{\delta G_m}{\delta x_{\mathrm{Al}}}\right)=\nabla\left(\frac{\partial G_m}{\partial x_{\mathrm{Al}}}\right)=\frac{\partial^2 G_m}{\partial x_{\mathrm{Al}}^2}\nabla x_{\mathrm{Al}}+\frac{\partial^2 G_m}{\partial x_{\mathrm{Al}}\partial\phi}\nabla\phi. \tag{34}$$

Thus, we can identify the diffusion coefficient $D_{\mathrm{Al}}=L''\frac{\partial^2 G_m}{\partial x_{\mathrm{Al}}^2}$ and therefore

$$\dot{x}_{\mathrm{Al}}=\nabla\cdot\left[M_{\mathrm{Al}}x_{\mathrm{Al}}(1-x_{Al})\left(\frac{\partial^2 G_m}{\partial x_{\mathrm{Al}}^2}\nabla x_{\mathrm{Al}}+\frac{\partial^2 G_m}{\partial x_{\mathrm{Al}}\partial\phi}\nabla\phi\right)\right] \tag{35}$$

There are two reasonable choices for M_{Al} at the interface:

$$M_{\mathrm{Al}}=M^{\alpha}_{\mathrm{Al}}(1-p(\phi))+M^{\gamma}_{\mathrm{Al}}p(\phi) \tag{36}$$

and

$$M_{\mathrm{Al}}=\left(\frac{M^{\gamma}_{\mathrm{Al}}}{M^{\alpha}_{\mathrm{Al}}}\right)^{p(\phi)}. \tag{37}$$

For the derivation we will use Eq. (36).

The derivatives of Eqs. (29)–(31):

$$\frac{\partial G^{\alpha}_m}{\partial x_{\mathrm{Al}}}=-{}^0G^{\gamma}_{\mathrm{Ti}}+{}^0G^{\gamma}_{\mathrm{Al}}+RT[\ln(x_{\mathrm{Al}})-\ln(1-x_{\mathrm{Al}})] \tag{38}$$
$$-x_{\mathrm{Al}}(G^{\alpha}_0+G^{\alpha}_1(1-2x_{\mathrm{Al}}))+(1-x_{\mathrm{Al}})$$
$$(G^{\alpha}_0+G^{\alpha}_1(1-2x_{\mathrm{Al}}))-2x_{\mathrm{Al}}(1-x_{\mathrm{Al}})G^{\alpha}_1$$

$$\frac{\partial^2 G^{\alpha}_m}{\partial x_{\mathrm{Al}}^2}=\frac{RT}{x_{\mathrm{Al}}(1-x_{\mathrm{Al}})}-2(G^{\alpha}_0+3G^{\alpha}_1)+12G^{\alpha}_1x_{Al} \tag{39}$$

$$=\frac{RT}{x_{\mathrm{Al}}(1-x_{\mathrm{Al}})}+R^{\alpha} \tag{40}$$

$$\frac{\partial G^{\gamma}_{m,x_{\mathrm{Al}}>0.5}}{\partial x_{\mathrm{Al}}}=-{}^0G^{\gamma}_{\mathrm{Ti}}+{}^0G^{\gamma}_{\mathrm{Al}}+RT[(-\ln(1-2x_{\mathrm{Al}})- \tag{41}$$
$$-\ln(2x_{\mathrm{Al}})]+\frac{\partial A^{12}}{\partial x_{\mathrm{Al}}}x_{\mathrm{Al}}+A^{12}$$
$$+\frac{\partial A^{22}}{\partial x_{\mathrm{Al}}}(1-2x_{\mathrm{Al}})x_{\mathrm{Al}}+A^{22}(1-4x_{\mathrm{Al}})$$

$$\frac{\partial^2 G^{\gamma}_{m,x_{\mathrm{Al}}>0.5}}{\partial x_{\mathrm{Al}}^2}=\frac{RT}{(1-2x_{\mathrm{Al}}-1)x_{\mathrm{Al}}}+\frac{\partial^2 A^{12}}{\partial x_{\mathrm{Al}}^2}x_{\mathrm{Al}}+2\frac{\partial A^{12}}{\partial x_{\mathrm{Al}}} \tag{42}$$
$$+\frac{\partial^2 A^{22}}{\partial x_{\mathrm{Al}}^2}(1-2x_{\mathrm{Al}})x_{\mathrm{Al}}+2\frac{\partial A^{22}}{\partial x_{\mathrm{Al}}}(1-4x_{\mathrm{Al}})-4A^{22}$$
$$=\frac{RT}{(1-2x_{\mathrm{Al}}-1)x_{\mathrm{Al}}}+R^{\gamma}_{x_{\mathrm{Al}}\geqslant 0.5} \tag{43}$$

$$\frac{\partial G^{\gamma}_{m,x_{\mathrm{Al}}<0.5}}{\partial x_{\mathrm{Al}}}={}^0G^{\gamma}_{\mathrm{Ti}}+{}^0G^{\gamma}_{\mathrm{Al}}+RT[-\ln(2(1-x_{\mathrm{Al}})) \tag{44}$$
$$+\ln(2x_{\mathrm{Al}}-1)]+\frac{\partial A^{11}}{\partial x_{\mathrm{Al}}}(1-x_{\mathrm{Al}})(2x_{\mathrm{Al}}-1)$$
$$+A^{11}(3-4x_{\mathrm{Al}})+\frac{\partial A^{22}}{\partial x_{\mathrm{Al}}}(1-x_{\mathrm{Al}})-A^{22}$$

$$\frac{\partial^2 G^{\gamma}_{m,x_{\mathrm{Al}}<0.5}}{\partial x_{\mathrm{Al}}^2}=\frac{RT}{(1-x_{\mathrm{Al}})(2x_{\mathrm{Al}}-1)}+\frac{\partial^2 A^{11}}{\partial x_{\mathrm{Al}}^2}(1-x_{\mathrm{Al}})(2x_{\mathrm{Al}}-1)$$
$$+\frac{\partial A^{11}}{\partial x_{\mathrm{Al}}}(3-4x_{\mathrm{Al}})-4A^{11}+\frac{\partial^2 A^{22}}{\partial x_{\mathrm{Al}}^2}(1-x_{\mathrm{Al}})-2\frac{\partial A^{22}}{\partial x_{\mathrm{Al}}} \tag{45}$$
$$=\frac{RT}{x_{\mathrm{Al}}(1-2x_{\mathrm{Al}})}+R^{\gamma}_{x_{\mathrm{Al}}<0.5} \tag{46}$$

In Eqs. (40), (43) and (46) the term R^i denotes a simplification for all the other terms.

The problem of Eqs. (43) and (46) is that the first term of the right-hand side is not identical. We therefore have to modify $L^{''}$ in the following way

$$L''=M_{x_{\mathrm{Al}}}[(1-p(\phi))x_{\mathrm{Al}}(1-x_{\mathrm{Al}})+p(\phi)(1-x_{\mathrm{Al}})$$
$$\times(2x_{\mathrm{Al}}-1)]\ \ for x_{\mathrm{Al}}<0.5 \tag{47}$$
$$L''=M_{x_{\mathrm{Al}}}[(1-p(\phi))x_{\mathrm{Al}}(1-x_{\mathrm{Al}})+p(\phi)(1-x_{\mathrm{Al}})$$
$$\times(1-2x_{\mathrm{Al}})x_{\mathrm{Al}}]\ \ for x_{\mathrm{Al}}\geqslant 0.5 \tag{48}$$

Finally the diffusion Eq. (35) for $x_{\mathrm{Al}}<0.5$

$$\dot{x}_{\mathrm{Al}}=\nabla\cdot[M_{\mathrm{Al}}x_{\mathrm{Al}}(1-x_{\mathrm{Al}})(1-p(\phi))+p(\phi)x_{\mathrm{Al}}(1-2x_{\mathrm{Al}})]$$
$$\cdot\left\{\left[(1-p(\phi))\left(\frac{RT}{x_{\mathrm{Al}}(1-x_{\mathrm{Al}})}+R^{\alpha}\right)\right.\right.$$
$$+p(\phi)\left(\frac{RT}{x_{\mathrm{Al}}(1-2x_{\mathrm{Al}})}+R^{\gamma}_{x_{\mathrm{Al}}<0.5}\right)\nabla x_{\mathrm{Al}}$$
$$\left.\left.+30g(\phi)\left(-\frac{\partial G^{\alpha}_m}{\partial x_{\mathrm{Al}}}+-\frac{\partial G^{\gamma}_m}{\partial x_{\mathrm{Al}}}\right)\nabla\phi\right]\right\} \tag{49}$$

Thus

$$\dot{x}_{\mathrm{Al}}=\nabla\cdot\left\{RTM_{\mathrm{Al}}\left\{(1-p(\phi))^2\left(1+\frac{R^{\alpha}}{RT}\right)x_{\mathrm{Al}}(1-x_{\mathrm{Al}})\right.\right.$$
$$+p^2(\phi)\left(1+\frac{R^{\gamma}}{RT}x_{\mathrm{Al}}(1-2x_{\mathrm{Al}})\right)$$
$$+(1-p(\phi))p(\phi)\left(\frac{1-x_{\mathrm{Al}}}{1-2x_{\mathrm{Al}}}+\frac{R^{\gamma}}{RT}x_{\mathrm{Al}}(1-x_{\mathrm{Al}})\right.$$
$$\left.\left.+\frac{1-2x_{\mathrm{Al}}}{1-x_{\mathrm{Al}}}\frac{R^{\alpha}}{RT}x_{\mathrm{Al}}(1-2x_{\mathrm{Al}})\right)\right\}\nabla x_{\mathrm{Al}}$$
$$+RTM_{\mathrm{Al}}((1-p(\phi))x_{\mathrm{Al}}(1-x_{\mathrm{Al}})$$
$$+p(\phi)x_{\mathrm{Al}}(1-2x_{\mathrm{Al}}))$$
$$\times\left[30g(\phi)\left(-\frac{1}{RT}\frac{\partial G^{\alpha}_m}{\partial x_{\mathrm{Al}}}+\frac{\partial G^{\gamma}_m}{\partial x_{\mathrm{Al}}}\frac{1}{RT}\right)\right]\nabla\phi\Big\} \tag{50}$$

In order to perform simulations we have non-dimensionalized the governing equations with $x\rightarrow xl$, where $l=\delta$ is the reference length. The time was non-dimensionalized with $t\rightarrow tl^2/D$, where D is a reference diffusion coefficient and can be taken as $D=RTM^{\alpha}_{\mathrm{Al}}$. Accordingly the free energy and the hump were non-dimensionalized as $\widetilde{G}=G/RT$ and $\widetilde{W}=W/RT$. Thus, the phase field equation becomes

$$\frac{D}{l^2}\dot{\phi}=M_{\phi}\varepsilon^2\frac{1}{l^2}\nabla^2\phi+M_{\phi}RT(30g(\phi)(\widetilde{G}^{\alpha}_m-\widetilde{G}^{\gamma}_m)-g'(\phi)\widetilde{W}) \tag{51}$$

and so

$$\dot{\phi}=\widetilde{M}_{\phi}\widetilde{\varepsilon}^2\nabla^2\phi+\widetilde{M}_{\phi}RT(30g(\phi)(\widetilde{G}^{\alpha}_m-\widetilde{G}^{\gamma}_m)-g'(\phi)\widetilde{W}) \tag{52}$$

with $\widetilde{M}_{\phi}=l^2M_{\phi}/D$ and $\widetilde{\varepsilon}^2=\varepsilon^2/l^2$.

The diffusion equation becomes

$$\frac{D}{l^2}\dot{x}_{\mathrm{Al}} = \frac{D}{l^2}\nabla\cdot\left[\frac{RTM_{\mathrm{Al}}}{D}(\{\ldots\}\nabla x_{\mathrm{Al}} + \{\ldots\} \times \left\{30g(\phi)\left(\frac{\partial\widetilde{G}_m^{\gamma}}{\partial x_{\mathrm{Al}}} + \frac{\partial\widetilde{G}_m^{\alpha}}{\partial x_{\mathrm{Al}}}\right)\right\}\nabla\phi\right)\right] \tag{53}$$

References

[1] Liu CT, Wright JL, Deevi SC. Mater Sci Eng A 2002;329–331:416–23.
[2] Clemens H, Kestler H. Adv Eng Mater 2000;2(9):551–70.
[3] Appel F, Brossmann U, Christoph U, Eggert S, Janschek P, Lorenz U, et al. Adv Eng Mater 2000;2(11):669–720.
[4] Wu X. Internet 2006;14:1114–22.
[5] Denquin A, Naka S. Acta Mater 1996;44(1):343–52.
[6] Denquin A, Naka S. Acta Mater 1996;44(1):353–6.
[7] Zghal S, Thomas M, Naka S, Finel A, Couret A. Acta Mater 2005;53:2653–64.
[8] Zghal S, Thomas M, Couret A. Internet 2005;13:1008–13.
[9] Dey SR, Hazotte A, Bouzy E, Naka S. Acta Mater 2005;53:3783–94.
[10] Perez-Bravo M, Madariaga I, Ostolaza K, Tello M. Scripta Mater 2005;53:1141–6.
[11] Guo J, Li X, Su Y, Wu S, Li B, Fu H. Internet 2005;13:275–9.
[12] Kim SG, Kim WT, Suzuki T. Phys Rev E 1999;60:7186–97.
[13] Wen YH, Chen LQ, Hazzledine PM, Wang Y. Acta Mater 2001;49:2341–53.
[14] Katzaraov I, Malinov S, Sha W. Acta Mater. 2006;54:453–63.
[15] Wang Y, Khachaturyan AG. Scripta Metall Mater 1994;31(10):1425–30.
[16] Loginova I, Odquist J, Amberg G, Ågren J. Acta Mater 2003;51:1327–39.
[17] Loginova I, Amberg G, Ågren J. Acta Mater 2004;52:4055–63.
[18] Kim SG, Kim WT, Suzuki T. Phys Rev E 1998;58:3316–23.
[19] Boettinger WJ, Warren JA, Beckermann C, Karma A. Annu Rev Mater Res 2002;32:163–94.
[20] Huang SC, Siemers PA. Metal Mater Trans A 1989;20(10): 1899–906.
[21] McCullough C, Valencia JJ, Levi CG, Mehrabian R. Acta Metall 1989;37:1321–36.
[22] Shibata K, Sato T, Ohira G. J Crystal Growth 1978;44:435–45.
[23] Kaufman L, Nesor H. CALPHAD 1978;4:325–48.
[24] Kattner UR, Lin J-C, Chang YA. Metall Trans A 1992;23:2081–90.
[25] Zhang F, Chen SL, Chang YA, Kattner UR. Internet 1997;5:471–82.
[26] Ohnuma I, Fujita Y, Mitsui H, Ishikawa K, Kainuma R, Ishida K. Acta Mater 2000;48:3113–23.
[27] Chen SL, Kao CR, Chang YA. Internet 1995;3:233–42.
[28] Dinsdale AT. CALPHAD 1991;15:317–425.
[29] Kattner UR. private communications.
[30] Provatas N, Goldenfeld N, Dantzig J. Phys Rev Lett 1998;80:3308–11.
[31] Finite Element package FEMLego. Available from: <http://www2.mech.kth.se/~gustava/femLego/>.
[32] Lan CW, Chang YC, Shih CJ. Acta Mater 2003;51:1857–69.
[33] Singer I, Singer HM. 2006, unpublished research.
[34] Slavov V, Dimova S, Iliev O. LSSC 2003, LNCS2907 2004: 404–411.
[35] Biben T, Kassner K, Misbah C. Phys Rev E 2005;72:041921.
[36] Ågren J. Acta Metall 1982;30:841–51.
[37] Hillert M. Phase equilibria, phase diagrams and phase transformations. Cambridge: Cambridge University Press; 1998.
[38] Sprengel W, Nakjima H, Oikawa H. Mater Sci Eng A 1996;213:45–50.
[39] Herzig Chr, Przeorski T, Mishin Y. Internet 1999;7:389–404.
[40] Mishin Y, Herzig Chr. Acta Mater 2000;48:589–623.
[41] Herzig Chr, Wilger T, Przeorski T, Hisker F, Divinski S. Internet 2001;9:431–2.
[42] Hillert M. Metall Mater Trans A 2002;33:2299–308.
[43] Veeraraghavan D, Wang P, Vasudevan VK. Acta Mater 1999;47:3313–30.
[44] Burke JE, Turnbull D. Prog Metal Phys 1952;3:220–44.
[45] Hillert M. Metall Trans A 1975;6:5–19.